Validation of Aura Microwave Limb Sounder OH and HO_2 Measurements

H. M. Pickett, B. J. Drouin, T. Canty, R. J. Salawitch, R. A. Fuller, V. S. Perun, N. J. Livessey, J. W. Waters, R. A. Stachnik, S. P. Sander, and W. A. Traub

Jet Propulsion Laboratory, Calif. Inst. of Tech., Pasadena, California, USA

K. W. Jucks

Harvard-Smithsonian Center for Astrophysics, Cambridge, Massachusetts, USA

K. Minschwaner

New Mexico Institute of Mining and Technology, Socorro, New Mexico, USA

Abstract. The Microwave Limb Sounder (MLS) instrument on the Aura satellite measures both OH and HO_2 radicals globally. This paper describes the precision and systematic errors of the MLS version v2.2 of the retrieval software. Estimated systematic errors are less than 8% for OH over 32–0.003 hPa and HO_2 over 6.8–0.21 hPa. Comparison of measurements from MLS OH and HO_2 profiles and 3 balloon-based instruments show good agreement among themselves and with a photochemical model. Similar good agreement is found with ground-based measurements of OH column. Middle Atmosphere High Resolution Spectrographic Investigation (MAHRSI) measurements of OH are smaller than MLS measurements by 20% at 70 km, are the same near 50 km., and are 50% larger near 42 km.

Introduction

The Aura satellite was launched on July 15, 2004 into a sun-synchronous near-polar orbit. The Microwave Limb Sounder (MLS) instrument on the Aura satellite measures the hydroxyl radical (OH) and the peroxy radical (HO_2) both day and night [*Waters et al.*, 2006]. Details on the THz module that measures OH and its calibration are given in *Pickett* [2006b]. Details on the retrieval algorithms are given by *Livesey et al.* [2006]. Early validation of OH and HO_2 with balloon-borne remote sensing instruments are given in *Pickett, et al* [2006a]. Early validation of other molecules measured by MLS are given in *Froidevaux et al.* [2006]. The current version of the MLS retrieval software is v2.2 and is the current production software. All the data taken from launch to February 2007 has been processed with the earlier version v1.5. The data since launch will be reprocessed with version v2.2, but only selected days have been reprocessed thus far. However, unless otherwise stated, this paper will use version v2.2. A description of the differences between these two major versions as it relates to HO_x will be given below.

Odd hydrogen (HO_x=OH+HO_2+H) chemistry dom-

inates atmospheric ozone destruction at heights above 40 km and below 25 km. Observations of OH over 40–80 km from MAHRSI [*Conway et al.*, 2000] are not consistent with current chemical models. Photochemical models could not reconcile with MAHRSI data over 40–80 km using adjusted rate constants for known reactions, leading to the designation "HO_x dilemma." However, balloon-borne observations that are mostly sensitive to HO_x below 40 km agree better with photochemical models [*Jucks et al.*, 1998] and [*Canty et al.*, 2006]. MLS measurements of HO_x

MLS Measurements

Overview

The OH measurements are made with a THz receiver [*Pickett*, 2006a] that uses a gas laser as the local oscillator (*Mueller et al., submitted*). There are six receiver bands (15–20) in the THz receiver, each connected to a 25-channel filter-bank. The filters near the center of each band are 6 MHz wide, and the width increases to 96 MHz at ±575 MHz from band center. Four of these bands (15,16,18,19) are used to observe OH. In addition there are two receiver bands (17,20) that are used for pointing information. The frequencies of the target lines are shown in Table 1 and an example of the observed radiance is shown in Figure 1. The OH lines indicated in Table 1 are each split into 3 hyperfine components [*Blake et al., 1986*]. There is a THz a mixer for each of two different linear polarizations that provide simultaneous measurements to improve the OH signal to noise ratio. Bands 15-17 and bands 18-20 have perpendicular polarizations, with axes that are oriented $\sim 26^\circ$ from nadir. The Zeeman splitting is $\sim \pm 1$ MHz and, in the small splitting limit, the polarization differences can be shown to be proportional to the square of the ratio of the Zeeman shift to the Doppler width (6 MHz). Therefore, measurements from the two polarizations are fitted simultaneously by a model of unpolarized emission. Bands 16 and 19 have an O_3 line at the edge from witch an O_3 profile is retrieved. While the noise associated with this O_3 profile is large compared with the O_3 profile from the GHz bands, comparison of profiles with GHz O_3 gives added information on systematic errors.

The THz module retrieves pointing information from bands 17 and 20 using a magnetic dipole line of O_2 in the lower sideband and a strong line of O_3 in the upper sideband. Band 20 does not have a dedicated filter bank, but the filter-bank used nominally for 640-GHz N_2O can be switched to band 20. During instrument checkout shortly after launch, the band 20 performance

Table 1.

Figure 1.

was checked out successfully and bore-sight offsets were determined. Since then the instrument has been configured for N_2O measurements and band 20 data is not available. An example of the observed band 17 radiance is shown in Figure 2.

Figure 2.

The HO_2 measurements are made from two HO_2 lines in the 640 GHz radiometer each using a 11-channel mid-band filter-bank. These filter-banks are identical in design to the center channels of the standard 25-channel filter-bank and are embedded in the frequency space of other bands. Data from all the filer-banks in the 640 GHz radiometer are used to retrieve profiles for eight other molecules in addition to HO_2. An example of the observed radiance is shown in Figure 3. The HO_2 signal is only $\sim$ 1K and signal / noise is $\sim$ 3 after a zonal average over 120° latitude. Consequently 12 days of data are needed to obtain the same signal/noise over a 10° latitude range.

Figure 3.

A day–night HO_2 difference is required to reduce systematic errors to an acceptable level. This differencing works for altitudes below 0.03 hPa. Above this altitude there can be significant HO_2 at night due to the long reactive lifetimes of HO_x at these low pressures [*Pickett et al.*, 2006c], but use of data above this altitude is also not recommended because of undue influence of a priori profiles.

The MLS Level 2 data (retrieved geophysical parameters and diagnostics at the measurement locations along the suborbital track) are generated from input Level 1 data (calibrated radiances and engineering information) by the MLS data processing software. The MLS retrieval algorithms, described in detail by Livesey et al. [2006], are based on the standard optimal estimation method; they employ a two-dimensional approach that takes into account the fact that limb observations from consecutive scans cover significantly overlapping regions of the atmosphere. The results are reported in Level 2 Geophysical Product (L2GP) files, which are standard HDF-EOS version 5 files containing swaths in the Aura-wide standard format [Livesey et al., 2007, available from the MLS web site, http://mls.jpl.nasa.gov]. A separate L2GP file is produced for each standard MLS product for each day (00–24 UT).

Data Screening

Examples of the THz spectra and residuals for daytime are shown in Figures 1 and 2. To obtain radiance closure such as that shown in the Figures, it is essential to screen the data using 3 pieces of information from the L2GP swath structure:

1. Use only even values of STATUS. Profiles with

odd STATUS are flagged by the level 2 retrieval software for various errors that are described by other bits in the STATUS word (see Table 2).

2. Use only positive precision values. The precision field is flagged by the level-2 software with a negative sign when the estimated precision is 50% of the a priori precision. Negative precisions usually appear at the edge of the useful altitude range.

3. Use only scans with CONVERGENCE < 1.1. This field contains additional information on the success of the retrieval and compares the fit profiles to that expected by the linearized retrieval, with values around 1.0 typically indicating good convergence. A cutoff of 1.1 is a compromise between eliminating pathological non-converging fits and keeping fits that have adequately converged.

Over the pressure range of 32–10 hPa, one should use day–night differences to reduce biases. The recommended range for OH is 32–0.003 hPa.

Table 2.

An example of the spectra and residuals in the 640 GHz radiometer near the two HO_2 lines are shown in Figure 3. The radiance shown is a day–night difference. The data filtering procedure is identical to that for the THz OH retrievals. Recommended range for HO_2 is 21–0.03 hPa

Resolution and Precision

The resolution of the retrieved profiles is described by the averaging kernels. Because the level 2 processing uses a 2-dimensional retrieval, the averaging kernel has both a vertical component and a horizontal component in the direction of the line of sight. Perpendicular to the line of sight the spatial resolution is determined by the horizontal width of the antenna pattern and is 1.5 km (HO_2) to 2.5 km (OH). Because MLS only scans in the plane of the orbit, the Aura orbit limits the longitude sampling to 24°.

Figure 4 shows the OH averaging kernel for daytime at the equator. This kernel is representative of the daytime averaging kernels at latitudes $< 60°$. The vertical width of the averaging kernel at altitudes below 0.01 hPa is 2.5 km. The horizontal width of the averaging kernel is equivalent to a width of 1.5° (165 km) distance along the orbit. The changes in vertical resolution above 0.01 hPa are due mainly to use of a faster operational scan rate for tangent heights above 70 km.

Figure 4.

Figure 5 shows the HO_2 averaging kernel for daytime at the equator. The vertical width of the averaging kernel at altitudes below 0.1 hPa is 4 km. The horizontal width of the averaging kernel is 2–4 profiles or a

3-6° distance along the orbit. In software version v2.2, smoothing of the profile was applied to reduce indeterminacy in the fit that was manifested in v1.5 as a vertical oscillation in the profile. The effect of the smoothing in v2.2 is to broaden the vertical averaging kernels to a width of 4 km and to broaden the horizontal averaging kernel by a factor of 2–4.

Figure 5.

A typical OH concentration profile and associated precision estimate is shown in Figure 6. The profile is shown both in volume mixing ratio (vmr) and density units. All MLS data are reported in vmr for consistency with the other retrieved molecular profiles. However, use of density units (10^6 cm^{-3}) reduces the apparent steep vertical gradient of HO_x allowing one to see the profile with more detail. Additionally, at THz frequencies the collisional line-width is approximately equal to the Doppler width at 1 hPa. At altitudes above 1 hPa Doppler broadening is dominant and the peak intensity of OH spectral absorption is proportional to density. (At altitudes below 1 hPa, the peak intensity is proportional to vmr.) The daytime OH density profile shows two peaks at $\sim$ 45 km and $\sim$ 75 km that are not as apparent in the vmr-based profiles. The night profile of OH exhibits the narrow layer at $\sim$ 82 km that has been described earlier [*Pickett et al.,* 2006c]. Precisions are such that an OH zonal average with a 10° latitude bin can be determined with better than 10% relative precision with one day of data (100 samples) over 21–0.01 hPa. With 4 days of data, the 10% precision limits can be extended to 32–0.0046 hPa.

Figure 6.

A typical HO_2 concentration profile and associated precision estimate is shown in Figure 7. The profile is shown both in volume mixing ratio (vmr) and density units. Precisions are such that a HO_2 zonal average with a 10° latitude bin can be determined with better than 10% relative precision from with 20 days of data (2000 samples) over 21–0.032 hPa.

Figure 7.

Expected Accuracy and Error characterization

A major component of the validation of MLS data is the quantification of the various sources of systematic uncertainty. Systematic uncertainties arise from instrumental issues: e.g., radiometric calibration, field of view characterization, spectroscopic uncertainty, and approximations in the retrieval formulation and implementation. This section summarizes the relevant results of a comprehensive quantification of these uncertainties that was performed for all MLS products. More information on this assessment is given in Appendix A of *Read et al.* (*this issue*) and repeated in the supplementary material of this paper.

The impact on MLS measurements of radiance (or pointing where appropriate) of each identified source of systematic uncertainty has been quantified and modeled. These modeled impacts correspond to either 2-σ estimates of uncertainties in the relevant parameters, or an estimate of their maximum reasonable errors based on instrument knowledge and/or design requirements. The effect of these perturbations on retrieved MLS products has been quantified for each source of uncertainty by one of two methods.

In the first method, sets of modeled errors corresponding to the possible magnitude of each uncertainty have been applied to simulated MLS cloud-free radiances, based on a model atmosphere, for a whole day of MLS observations. These sets of perturbed radiances have then been run through the routine MLS data processing algorithms, and the differences between these runs and the results of the 'unperturbed' run have been used to quantify the systematic uncertainty in each case. The impact of the perturbations varies from product to product and among uncertainty sources. Although the term 'systematic uncertainty' is often associated with consistent additive and/or multiplicative biases, many sources of 'systematic' uncertainty in the MLS measurement system give rise to additional scatter in the products. For example, although an error in the O_3 spectroscopy is a bias on the fundamental parameter, it has an effect on the retrievals of species with weaker signals (e.g., HNO_3 that is dependent on the amount and morphology of atmospheric ozone. The extent to which such terms can be expected to average down is estimated to first order by these 'full up studies' through their separate consideration of the bias and scatter each source of uncertainty introduces into the data. The difference between the retrieved product in the unperturbed run and the original 'truth' model atmosphere is taken as a measure of uncertainties due to retrieval formulation and numerics.

In the second method, the potential impact of some remaining (typically small) systematic uncertainties has been quantified through calculations based on simplified models of the MLS measurement system [see Read et al., submitted, 2007]. Unlike the 'full up studies', these calculations only provide estimates of 'gain uncertainty' (i.e., possible multiplicative error) introduced by the source in question. This approach does not quantify possible biases or additional scatter for these minor sources of uncertainty.

Finally, although the MLS observations are unaffected by thin cirrus clouds or stratospheric aerosols, thick clouds associated with deep convection can have

an impact on the MLS radiances. The MLS Level 2 data processing algorithms discard or downplay radiances identified (through comparison with predictions from a clear-sky model) as being strongly affected by clouds [*Livesey et al.*, 2006]. The contribution of cloud effects to the systematic uncertainty, both from the presence of clouds not thick enough to be screened out by the cloud filtering and from the loss of information through omission of cloud-impacted radiances, has been quantified by adding scattering from a representative cloud field to the simulated radiances and comparing retrievals based on these radiances to the unperturbed results. The cloud-induced effects shown in Figures 8 and 10 are estimated by considering only the cloudy profiles (as defined by the known amount of cloud in the 'truth' field). The contribution of clouds to HO_x systematic errors is negligible in part because the low altitude limit of 31–22 hPa is above the altitudes expected for thick clouds.

The estimated impacts of the systematic errors on OH are summarized in Figure 8. The largest category of errors contributing to the systematic bias errors is the radiometric and spectral calibration category. The two biggest contributors to this category are sideband fraction and gain compression. The contribution from these sources is approximately equal. The multiplicative errors are estimated to be less than 8% below 0.01 hPa. The dominant contributor to the slope error above 0.01 hPa is sideband fraction. The size of the OH errors relative to a typical profile can be seen by using a profile such as that in Figure 6.

An independent measure of the effect of sideband fraction uncertainty is to compare O_3 retrieved from the THz radiometer with that retrieved from the GHz radiometers. A comparison given by *Froidevaux et al.* (*this issue*) shows that the ratio of the O_3 concentrations is unity within 5% over 1–32 hPa. The uncertainty in OH due to sideband fraction should be the same as the uncertainty in the O_3(THz)/O_3(GHz) ratio. A complicating factor is that O_3(THz) line in bands 16 and 19 has a much stronger temperature dependence than O_3(GHz) lines. The calculated ratio of absorption coefficients changes by 1.7%/K, so the effect of temperature on the ozone ratio is small but not negligible.

Figure 8.

An independent view of the effect of a priori assumptions can be determined by synthetic calculations of radiance. It is important to have several measures of the contribution of a priori assumptions to the data. Figure 9 shows an example of such a calculation. Here the night a priori profile contributes 7% to the output data at 0.0068 hPa. The large daytime peak in the

a priori at 0.03 hPa shows no impact on differences between the assumed profile and the retrieved profile and the amount of a priori mixing is even smaller than at higher altitudes.

Figure 9.

The estimated impacts of the systematic errors on HO_2 are summarized in Figure 10. The largest category of errors contributing to the bias is the radiometric and spectral calibration category. The two biggest contributors to this category are sideband fraction and gain compression. The contribution from these sources is approximately equal. Both contribute to the low altitude peak in bias and standard deviation. The slope error has a peak at 10 hPa due to a priori and radiometric numerics. The slope error above 0.1 hPa is due to filter position uncertainty. The size of the HO_2 systematic errors relative to a typical profile can be seen using Figure 7.

Figure 10.

The effect of a priori assumptions can also have an important effect on the HO_2 data. Figure 11 shows a retrieval that uses synthetic radiance derived from an input profile that is constant above 0.1 hPa. The a priori concentration profile is zero throughout. The retrieval tracks the input profile up to 0.1 hPa. For altitudes above 0.032 hPa there is at least 20% a priori contamination.

Figure 11.

Differences between software versions v2.2 and and v1.5

For the THz radiometer data in v2.2, the first step for level-1 calibration of MLS emission is to calibrate the data using a procedure that is a slight modification from the calibration described in *Pickett*[2006a] for v1.5. The need for calibration change was found by examining the on-orbit variation of gain as a function of orbital phase. The gain has an approximately sinusoidal dependence on orbital phase that is 2–4% of the average value with a magnitude that depends on the filter channel. The gain change is needed to account for small thermal effects on gain over the orbit. In v1.5, the gain was assumed to be constant over the orbit. In v2.2, the fitted gain is now assumed to have an additional sinusoidal dependence on orbital phase as well as the constant dependence assumed in v1.51. The second change in v2.2 calibration is that the radiometric zero is derived only from the space view, whereas before in v1.5 it was derived from both the space view and the calibration target. This change makes small radiances less sensitive to assumptions about the gain. Both changes are part of v2.2 level 1 processing. The result is that the OH radiance has better calibration, improving accuracy by as much as 2%.

In the OH level 2 v1.5 retrieval, the profiles were fitted to a pressure level interval of 3/decade above 0.1 hPa and 6/decade at lower altitudes. In v2.2 the profile sampling is 6/decade over the whole altitude range. There are many beneficial changes in OH above 50 km as can be seen in Figure 12. The profiles are smoother, have uniform pressure resolution, and have much fewer instances of negative concentration. In the stratosphere, OH fits are less subject to convergence problems in part because the iteration limit has been increased from 4 to 6.

Figure 12.

The main change for HO_2 is that there is more smoothing applied in this version. In v1.5, no effective smoothing was applied and the profiles tended to have a small but significant oscillation in concentration with height. This kind of behavior is often an indication the retrieval fitting is almost indeterminant, and the smoothing in v2.2 is effective in reducing this problem. The effect of smoothing at altitudes below 60 km is to broaden the averaging kernel to 4 km FWHM in the vertical and as much as 6 degrees along the track. Because of smoothing, precisions are no longer flagged negative above 60 km (0.1 hPa) but it is estimated that there is at least 20% a priori contamination for altitudes above 0.032 hPa (see above).

The second change for v2.2 was to set the HO_2 a priori concentration to zero. The v1.5 HO_2 a priori concentrations were based on the results of model calculations. This change was made to avoid potential artifacts due to the a priori assumptions.

Comparisons with other Data Sources

Comparison with Balloon-borne Instruments

The Balloon OH instrument (BOH), the Far Infrared Spectrometer (FIRS-2) instrument, and the Submillimeter Limb Sounder (SLS) were launched on a common balloon gondola on September 20, 2005, from Ft. Sumner, NM (latitude = 34.5° and longitude = −104°) and stayed aloft at ∼38 km for nearly 24 hours. The BOH instrument is a heterodyne limb-viewing thermal emission instrument that is functionally identical to the THz module on MLS [*Pickett,* 2006b] and only measures OH. The FIRS-2 instrument is a thermal emission far-infrared Fourier transform spectrometer developed at the Smithsonian Astrophysical Observatory [*Jucks et al.*, 1998]. It measures OH and HO_2 in the far infrared using multiple lines. SLS [*Stacknik et al.*, 1992] is a cryogenic heterodyne instrument that measures atmospheric radiance in the same spectral region as the MLS 640 GHz radiometer. One of the molecules measured by

SLS is HO_2. The results of all these measurements are summarized in Figure 13 along with a calculated profile from a photochemical model.

The balloon instruments all use limb sounding to increase the effective path length for tangent heights below the balloon altitude. The path lengths for layers above the balloon are an order of magnitude smaller than near the tangent height. Accordingly, the balloon instruments have only 1-2 independent pieces of information above the balloon. The dashed lines for the profile show what has been assumed for each of the balloon retrievals. In all cases the error bars are 1 σ. It can be seen that there is agreement among the instruments to 15%, but there significant differences between MLS OH and the two balloon-borne instruments at 40 km. The differences are smaller for the September 2004 balloon flight [*Pickett et al.*, 2006a].

Figure 13.

The HO_2 measurements overlap with the two balloon measurements within a combined experimental error of 20%. The precision for day–night differences has been multiplied by $3^{1/2}$ to account for the effects of the width of the horizontal averaging kernel (3 scans). There is no evidence that multiplicative systematic errors are as large as is shown in Figure 10.

The photochemical model is described by *Canty et al.* [2006]. Shown here is model C that uses adjustments of the OH + O rate to the *Smith and Stewart* [1994] value and a 20% increase in the OH + HO_2 rate. These two changes in rate constants were made to improve agreement between the model and measurements of OH and HO_2 below 40 km. The photochemical model constrains water and ozone to average values from MLS. Figure 13 shows that MLS and the model agree within the MLS precision. The comparison between the model and MLS can be made quantitative by using the χ^2 statistic. Figure 14 shows χ^2 for the the two balloon flight days and both versions v1.5 and v2.2 of the software. Model C was used for all comparisons. There is clearly significant improvement with versions.

Figure 14.

Comparison with Ground-based Column Measurements

At the time of the September 23, 2004 balloon flight, both the PEPSIOS instrument [Minschwaner et al, 2003] and the FTUVS instrument [*Cageao, et al.*, 2001] were observing the OH column in absorption against the Sun at 308 nm. The PEPSIOS instrument was located in Socorro, New Mexico, USA and the FTUVS was located at Table Mountain, California, USA. The observations are shown in Figure 15. The model in the dashed line is model C described above. The solid line is JPL06

rate constants [*Sander, et al.*, 2006] with no modification and the dotted line is JPL06 with only with adjustment of the OH + O rate to the *Smith and Stewart* [1994] value. BOH, FIRS-2, and MLS were corrected by adding both a tropospheric column using data of *Wennberg et al* [1998] and an additional contribution from the boundary layer [*Rohrer and Berresheim*, 2006]. The contribution from both these two sources of tropospheric OH is 7% of the total column. Both sources make similar contributions to the column. See the Appendix for further details.

Figure 15.

As with the balloon-based measurements, the agreement between different column measurement is within error estimates. The column can be a sensitive measure of OH in the stratosphere and mesosphere. Figure 16 shows the fractional contribution to the OH column for different altitude intervals. These fractions were determined from the actual MLS profile for September 23, 2004 above 20 km, modeled OH for 12–21 hPa, and the estimated contributions from the mesosphere and boundary layer. The mesospheric portion (and associated slow chemistry) is responsible for morning–afternoon asymmetries, while the largest contribution comes from the upper stratosphere near the 45 km peak in density. The MLS OH column for this day has increased in v2.2 by 9% compared to v1.5 due to improvements in the MLS mesospheric OH.

Figure 16.

Comparison with MAHRSI

The Middle Atmosphere High Resolution Spectrograph Investigation (MAHRSI) instrument flew on the Space Shuttle in 1994 [*Conway et al.*, 1999] and 1997 [*Conway et al.*, 2000]. We focus on the more recent flight because the observations were made at lower solar zenith angles (SZA) where the OH concentration is higher. We compare the MAHRSI data for August 15, 1999 with a zonal average of MLS data for September 7, 2005 over latitude range of 12–32°S and 33–53°N. This latitude range for the MLS zonal average was selected so that the SZA matched the MAHRSI range (32–49°). The comparison is shown in Figure 17. At the 42 km OH peak the MAHRSI value is 50% higher than MLS, and at the 70 km OH peak the MAHRSI values are 20% lower than MLS. Below 50 km, the MAHRSI measurements are challenging due to absorption of the OH signal by O_3 at 300 nm wavelength. While there may be significant systematic errors in the MAHRSI retrieval below 50 km due to O_3 absorption, there are smaller differences above 50 km of opposite sign. For both MAHRSI and MLS, the precision is better than 10% over 50–80 km and the differences are slightly larger

than the combined uncertainty.

Figure 17.

Summary and Conclusions

Version v2.2 is a substantial improvement from v1.5 particularly for mesospheric OH and stratospheric HO_2. Use of v1.5 HO_2 products can benefit from user-applied smoothing, but the internal smoothing in v2.2 is to be preferred because the averaging is done during the retrieval fit. OH in the upper stratosphere is very similar for the two versions.

A summary of the analysis of systematic errors is shown in Table 3 for OH and in Table 4 for HO_2. For OH, use of day–night differences are recommended for OH at altitudes $\leq$ 10 hPa because the bias uncertainty becomes zero when the differences are taken. The slope or scaling uncertainty for OH is <8% for altitudes below 0.01 hPa. Day–night differencing is not needed near 1 hPa because the bias is 0.3% of typical daytime OH densities. In addition, observed night concentrations of OH for 10–0.1 hPa are <1% of noontime tropical values. Use of day–night differences is recommended for HO_2 over the entire usable range of 21–0.03 hPa. The scaling errors for HO_2 are estimated to be larger, as much as 46% at 10 hPa. However, comparison with balloon measurements show that the actual systematic bias for HO_2 at 10 hPa is < 20%. Comparisons for both OH and HO_2 balloon measurements, models, and MLS measurements show good agreement, as do the column measurements.

MLS measurements of OH above 50 km agree with MAHRSI measurements within 20%. Below 50km, the differences are larger and may be due to systematic errors in modeling ozone absorption of the MAHRSI OH signal.

Table 3.

Table 4.

Acknowledgments. We wish to thank all who helped make the Aura HO_x measurements possible. Thanks to the Aura Project for their support throughout the years (before and after Aura launch), in particular M. Schoeberl, A. Douglass (also as co-chair of the Aura validation working group), E. Hilsenrath, and J. Joiner. We also acknowledge the support from NASA Headquarters, P. DeCola for MLS and Aura, and M. Kurylo, J. Gleason, B. Doddridge, and H. Maring, especially in relation to the Aura validation activities and campaign planning efforts. We are grateful to the Columbia Scientific Balloon Facility for launch services. Research at the Jet Propulsion Laboratory, California Institute of Technology, is performed under contract with the National Aeronautics and Space Administration.

References

Blake, G. A., J. Farhoomand, and H. M. Pickett (1986), The Far-infrared Rotational Spectrum od $X^2\Pi$ OH, *J. Mol. Spec., 115*, 226-228.

Cageao, R. P., J. F. Blavier, J. P. McGuire, Y. B. Jiang, V. Nemtchinov, F. P. Mills, and S. P. Sander (2001), High-resolution Fourier-transform ultraviolet-visible spectrometer for the measurement of atmospheric trace species: application to OH Source, *Applied Optics, 40*, 2024-2030.

Canty, T., H. M. Pickett, R. J. Salawitch, K. W. Jucks, W. A. Traub, J. W. Waters (2006), Stratospheric and mesospheric HO_x: results from Aura MLS and FIRS-2, *Geophys. Res. Lett., 33*, L12802.

Conway, R. R. *et al.* (1999), Middle Atmosphere High Resolution Spectrograph Investigation, *J. Geophys. Res. D*, *104*, 16327-16348.

Conway, R. R. *et al.* (2000), Satellite Observations of Upper Stratospheric and Mesospheric OH: The HO_x Dilemma, *Geophys. Res. Lett., 27*, 2613-2616.

Froidevaux, L. *et al.* (2006), Early Validation Analyses of Atmospheric Profiles from EOS MLS on the Aura Satellite, *IEEE Trans. Geosci. Remote Sensing, 44*, 1106-1121.

Jucks, K. W. *et al.* (1998), Observations of OH, HO_2, H_2O, and O_3 in the upper stratosphere: implications for HO_x photochemistry, *Geophys. Res. Lett., 25*(21), 3935-3938.

Livesey, N.J., W.V. Snyder, W.G. Read, and P.A. Wagner (2006), Retrieval algorithms for the EOS Microwave Limb Sounder (MLS) instrument, IEEE Trans. Geosci. Remote Sensing 44, 1144-1155.

Minschwaner K., T. Cant, C. R. Burnett (2003), Hydroxyl column abundance measurements: PEPSIOS instrumentation at the Fritz Peak Observatory and data analysis techniques, *J. Atmos. Solar-Terrest. Phys. 65*, 335-344

Pickett, H. M. (2006a), Microwave Limb Sounder THz Module on Aura, *IEEE Trans. Geosci. Remote Sensing, 44*, 1122-1130.

Pickett, H. M. *et al.* (2006b), Validation of Aura MLS HO_x measurements with remote-sensing balloon instruments, *Geophys. Res. Lett., 33*, L01808-L01811.

Pickett, H. M., W. G. Read, K. K. Lee,and Y. L. Yung (2006c), Observation of night OH in the mesosphere, *Geophys. Res. Lett., 33*, L19808.

Rohrer, R., and H. Berresheim (2006), Strong correlation between levels of troposhheric hydroxyls and solar utraviolet radiation, *Nature, 442*, 184-187.

Smith, I.W.M., and D.W.A. Stewart (1994), Low temperature kinetics of reactions between neutral free radicals, Rate constants for the reactions of OH radicals with N atoms ($103 \leq T/K \leq 294$) and with O atoms ($158 \leq T/K \leq 294$), *J. Chem. Soc. Faraday Trans., 90*, 3221-3227.

Stachnik, R. A., J. C. Hardy, J. A. Tarsala, J. W. Waters, and N. R. Erickson (1992), Submillimeter Wave Heterodyne Measurements of Stratospheric ClO, HCl, O_3, and HO_2 - 1St Results, *Geophys. Res. Lett., 19*, 1931-1934.

Sander, S.P., et al. (2006) Chemical kinetics and photochemi- cal data for use in atmospheric studies, evaluation number 15, JPL Publ., 06-2.

Waters, J. W., *et al.* (2006), The Earth Observing System Microwave Limb Sounder (EOS MLS) on the Aura Satellite, *IEEE Trans. Geosci. Remote Sensing, 44*, 1075-1092.

Wennberg, *et al.* (1998), Hydrogen Radicals, Nitrogen Radi-

cals, and the Production of O_3 in the Upper Troposphere, *Science, 279*, 49-53.

Herbert M. Pickett, B. J. Drouin, T. Canty, R. J. Salawitch, R. A. Fuller, V. S. Perun, N. J. Livessey, J. W. Waters, R. A. Stachnik, S. P. Sander, and W. A. Traub, Jet Propulsion Laboratory, 4800 Oak Grove Drive, Pasadena, CA 91109, USA. (herbert.m.pickett@jpl.nasa.gov)

K. W. Jucks, Harvard-Smithsonian Center for Astrophysics, 60 Garden St., Cambridge, MA 02138, USA.

K. Minschwaner, New Mexico Institute of Mining and Technology, Socorro, NM 87801, USA.

(Received _____)

Paper number .

PICKETT ET AL.: OH AND HO_2 VALIDATION

PICKETT ET AL.: OH AND HO_2 VALIDATION

PICKETT ET AL.: OH AND HO_2 VALIDATION

PICKETT ET AL.: OH AND HO_2 VALIDATION

PICKETT ET AL.: OH AND HO_2 VALIDATION

PICKETT ET AL.: OH AND HO_2 VALIDATION

PICKETT ET AL.: OH AND HO_2 VALIDATION

PICKETT ET AL.: OH AND HO_2 VALIDATION

PICKETT ET AL.: OH AND HO_2 VALIDATION

PICKETT ET AL.: OH AND HO_2 VALIDATION

PICKETT ET AL.: OH AND HO_2 VALIDATION

PICKETT ET AL.: OH AND HO_2 VALIDATION

PICKETT ET AL.: OH AND HO_2 VALIDATION

PICKETT ET AL.: OH AND HO_2 VALIDATION

PICKETT ET AL.: OH AND HO_2 VALIDATION

PICKETT ET AL.: OH AND HO_2 VALIDATION

PICKETT ET AL.: OH AND HO_2 VALIDATION

PICKETT ET AL.: OH AND HO_2 VALIDATION

PICKETT ET AL.: OH AND HO_2 VALIDATION

PICKETT ET AL.: OH AND HO_2 VALIDATION

PICKETT ET AL.: OH AND HO_2 VALIDATION

PICKETT ET AL.: OH AND HO_2 VALIDATION

PICKETT ET AL.: OH AND HO_2 VALIDATION

PICKETT ET AL.: OH AND HO_2 VALIDATION

PICKETT ET AL.: OH AND HO_2 VALIDATION

PICKETT ET AL.: OH AND HO_2 VALIDATION

PICKETT ET AL.: OH AND HO_2 VALIDATION

PICKETT ET AL.: OH AND HO_2 VALIDATION

PICKETT ET AL.: OH AND HO_2 VALIDATION

PICKETT ET AL.: OH AND HO_2 VALIDATION

Figure Captions

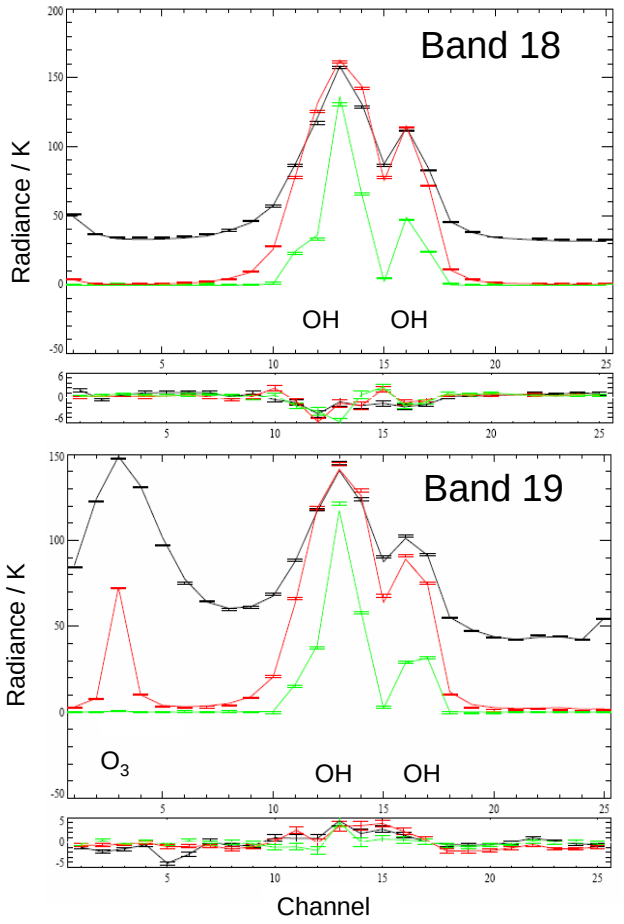

Figure 1. MLS radiance and residuals for Bands 18 and 19. The OH emission shown here is composed of 3 hyperfine components. Radiance is a daylight zonal average over latitudes from 60S to 60N for January 28, 2005. The radiance is nearly identical for Bands 15 and 16. The horizontal axis is the filter-bank channel number. The vertical axis is radiance in K. The black, red, and green plots are for tangent heights of 31.5, 40.7, and 62.5 km, respectively. The solid lines in the large panels are the predicted radiance and the center point of the error bars indicate the observed radiance. The small panels show the residuals for the observed minus calculated radiance.

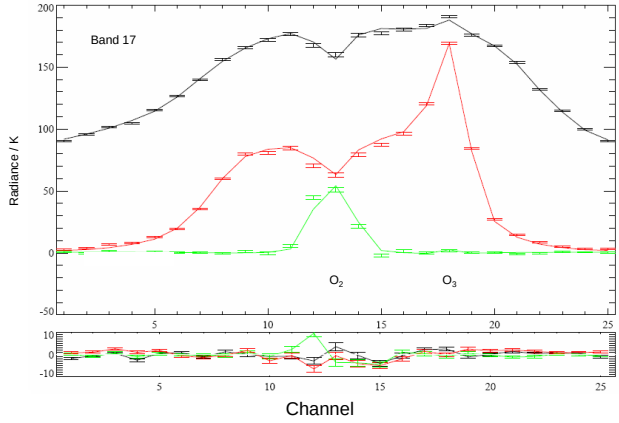

Figure 2. MLS radiance and residuals for Band 17. The O_2 emission is in the lower sideband and the THz O_3 emission is in the upper sideband. This band provides pointing information. Radiance shown here is a daylight zonal average over latitudes from 60S to 60N on January 28, 2005. See Figure 1 for further details.

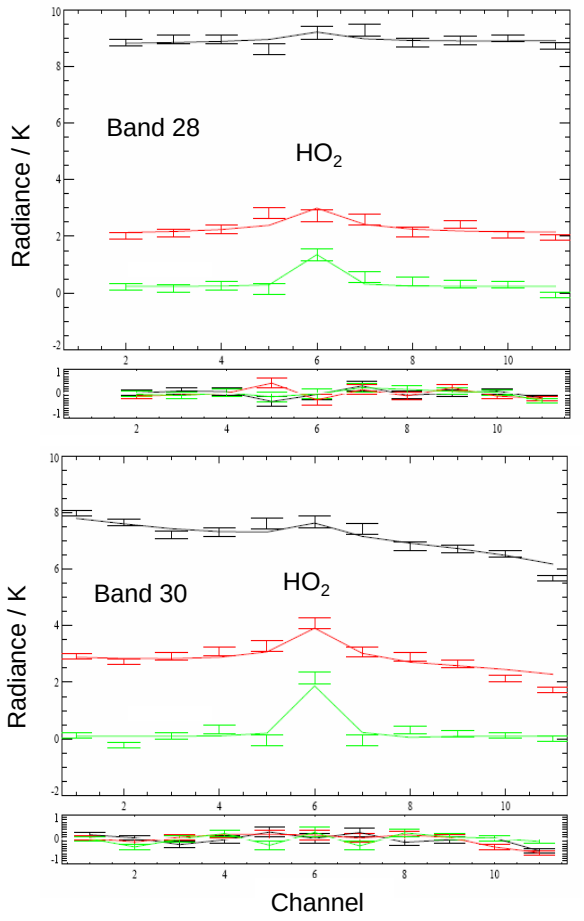

Figure 3. MLS radiance and residuals for Bands 28 and 30. The radiance shown is a day-night difference of zonal averages for latitudes from 60S to 60N on January 28, 2005. See Figure 1 for further details.

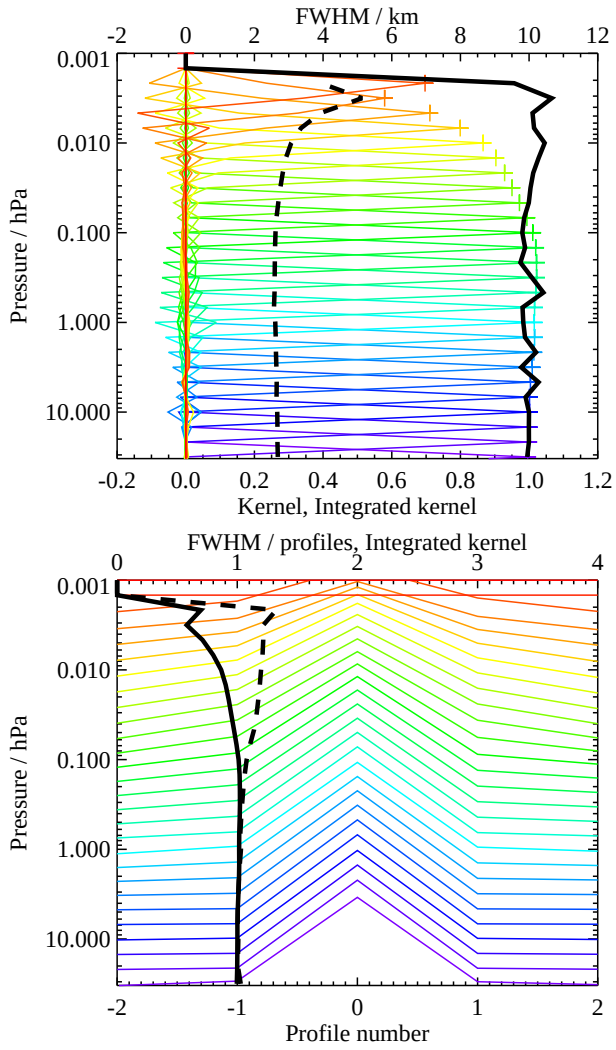

Figure 4. Vertical averaging kernels for OH are shown in the upper panel. The lower panel shows the horizontal averaging kernels along the line of sight. The individual colored plots are the averaging kernels. The dashed black line is the width of the kernel (top axes) and the solid black line is its integral (bottom axes).

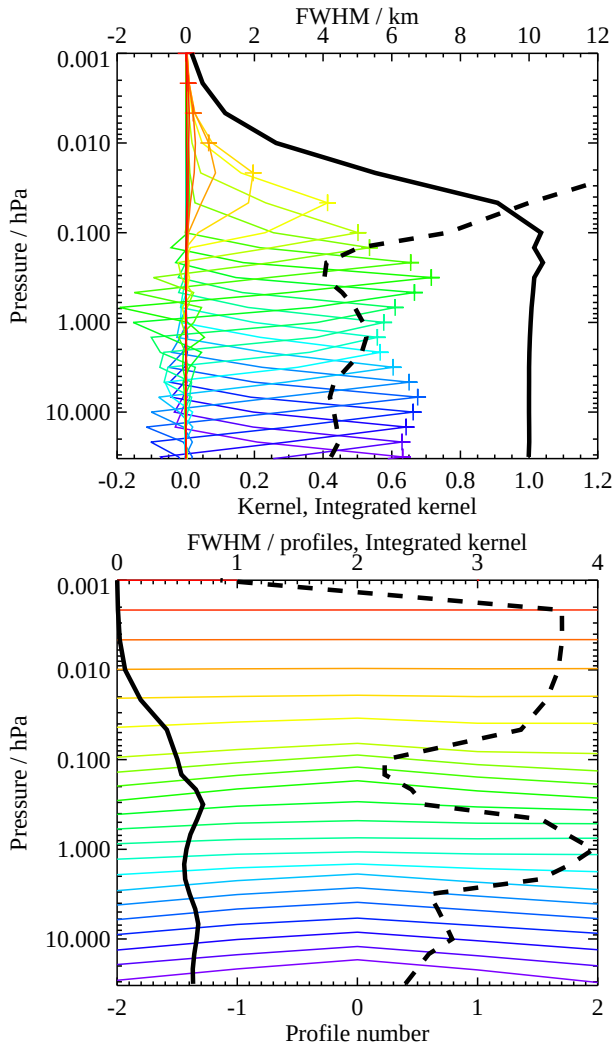

Figure 5. Averaging kernels for HO_2. See Figure 4 for further details.

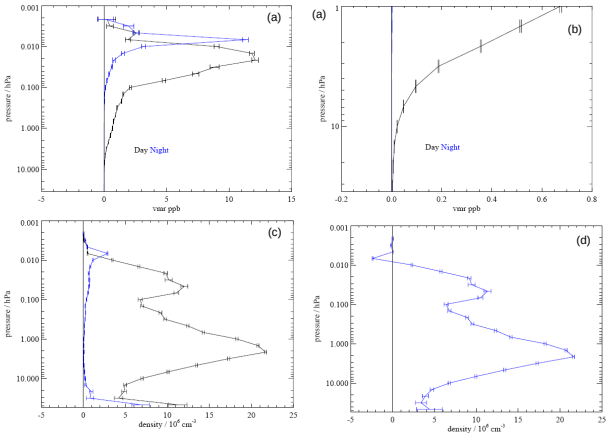

Figure 6. Zonal mean of Retrieved OH and its estimated precision (horizontal error bars) for September 20, 2005 averaged over 29N to 39N. The average includes 368 profiles. Panel (a) shows vmr vs. pressure for day (black) and night (blue) overpasses. Panel(b) shows the same data plotted for the stratosphere. Panel (c) shows the same data converted to density units. Panel(d) shows the day–night differences for the data in panel (c).

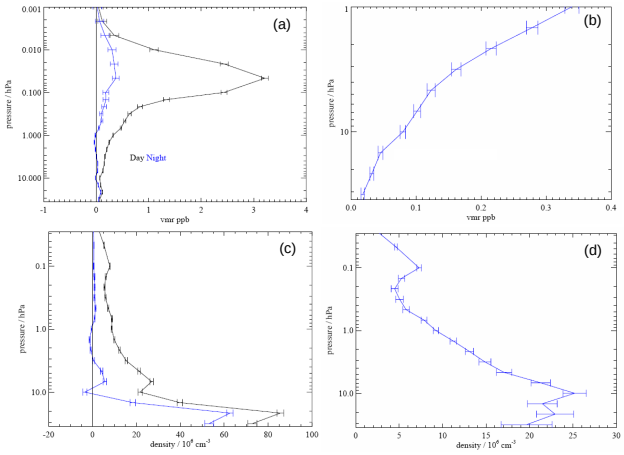

Figure 7. Zonal mean of Retrieved HO_2 and its precision for September 20, 2005 averaged over 29N to 39N. The average includes 2879 profiles. Panel (a) shows vmr vs. pressure for day (black) and night (blue) overpasses. Panel(b) shows the same data plotted as a day-night difference for the stratosphere. Panel (c) shows the same data converted to density units. Panel(d) shows the day–night differences for the data in panel (c).

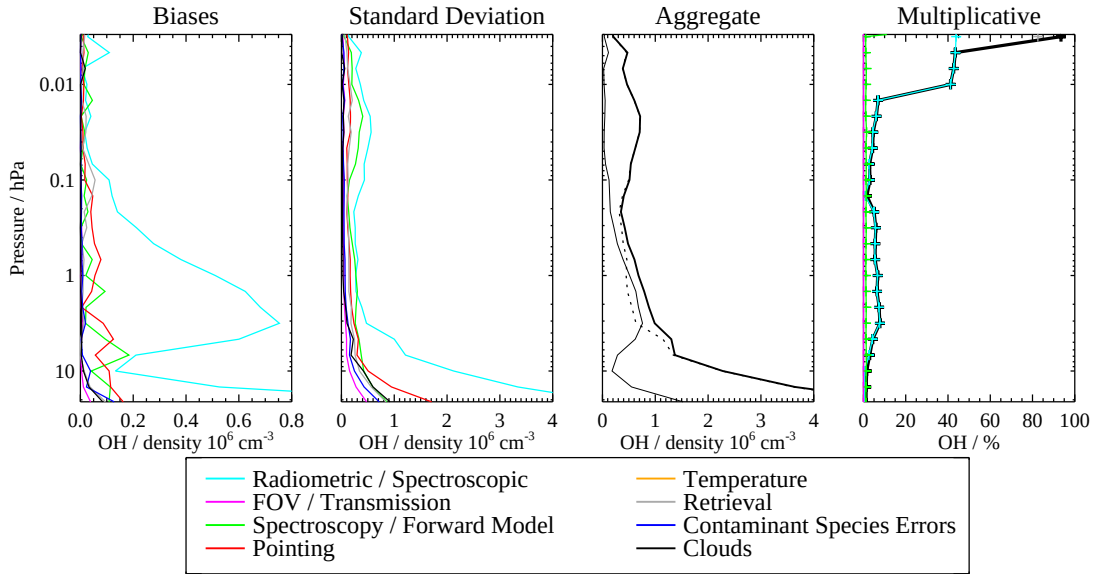

Figure 8. The estimated impact of various families of systematic errors on the MLS OH observations using nay–night differences. The first two panels show the (left) possible biases that are independent of concentration and (center left) additional scatter introduced by the various families of errors, with each family denoted by a different colored line. (Right center) the root sum squares (RSS) of all the possible biases (thin solid line), all the additional scatters (thin dotted line), and the RSS sum of the two (thick solid line). The right panel shows errors that are proportional to the concentration.

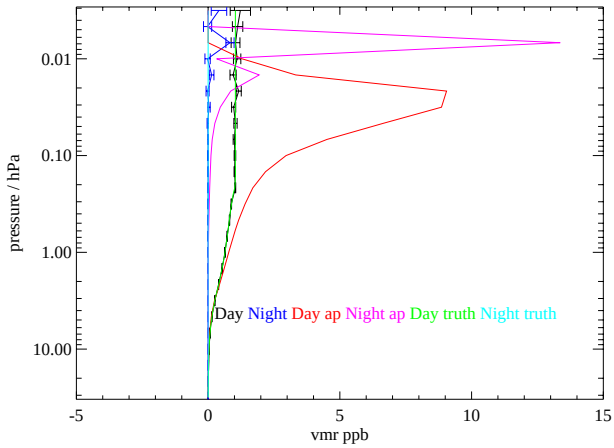

Figure 9. Retrieval results for synthetic OH profiles. The red line is the profile used to generate the synthetic daytime radiances. The red line is the daytime a priori profile.The black line with error bars is the retrieval output for the daytime profile and overlaps the green line. The error bars are the precision based on an estimated radiance uncertainty. No noise was added to the radiance. The night input profile (blue) was zero. The magenta line that peaks at 0.007 hPa is the night a priori profile. The blue line with error bars is the output retrieval for night.

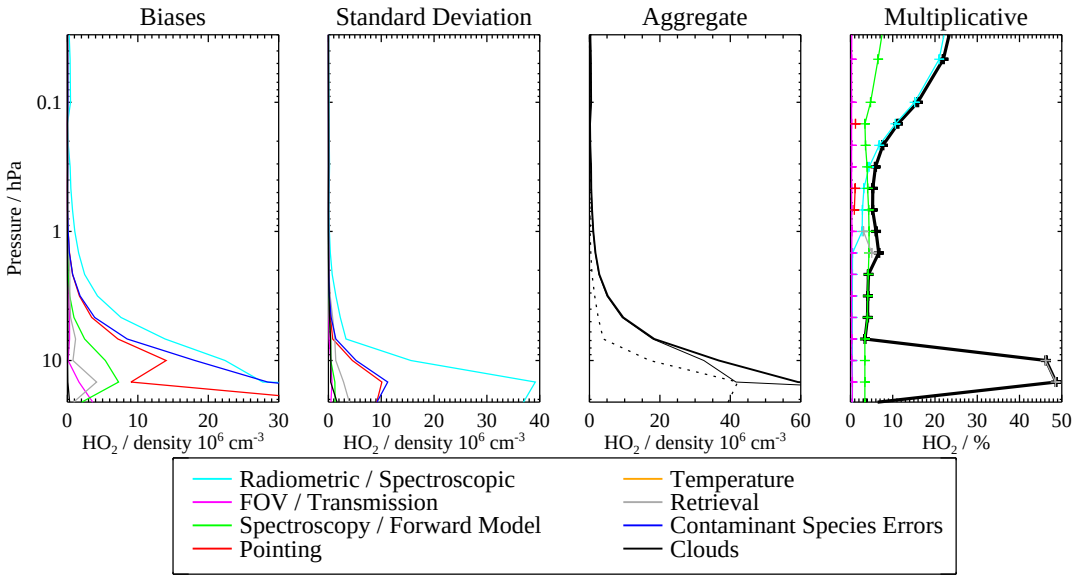

Figure 10. The estimated impact of various families of systematic errors on the MLS HO_2 observations of day–night differences. The first two panels show the (left) possible biases and (center) additional scatter introduced by the various families of errors, with each family denoted by a different colored line. For further details, see Figure 8

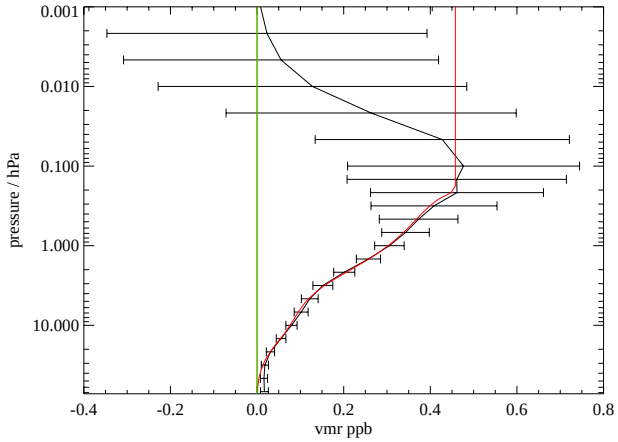

Figure 11. Retrieval results for synthetic HO_2 profiles. The red line is the profile used to generate the synthetic radiances. The black line is the retrieval output. The green line at zero is the a priori profile. The error bars are the precision based on a theoretical estimated radiance uncertainty. No noise was added to the radiance.

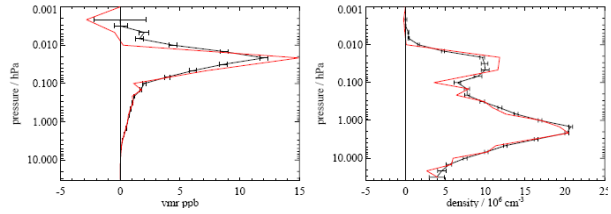

Figure 12. Comparison between v1.5 and v2.2 for MLS OH for September 23, 2004 zonally averaged over 29–39°N latitude. Red is version v1.5 and black is version v2.2. The same data is plotted in vmr (left panel) and density (right)

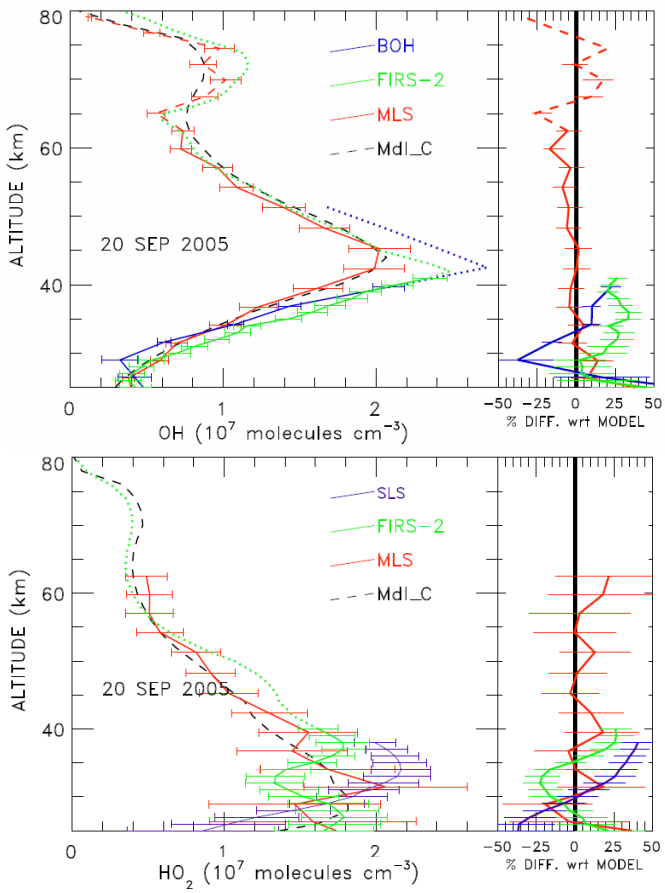

Figure 13. Balloon-borne HO_x observations for September 20, 2005 near Ft. Sumner, NM, USA. The top panel uses a zonal mean of MLS OH over a latitude range of 29–30°. The bottom panel uses a 9-day zonal mean of MLS HO_2 over the same latitude interval. The balloon data and model calculations are for the time of the MLS overpass.

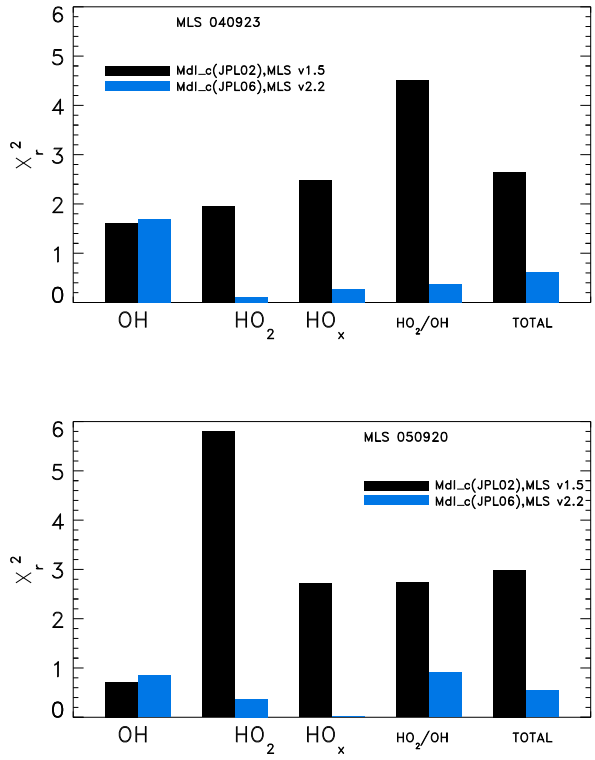

Figure 14. Comparison between model and MLS OH and HO_2 for September 23, 2004 and September 20, 2005. Black bars are v1.5 retrievals and blue bars are v2.2

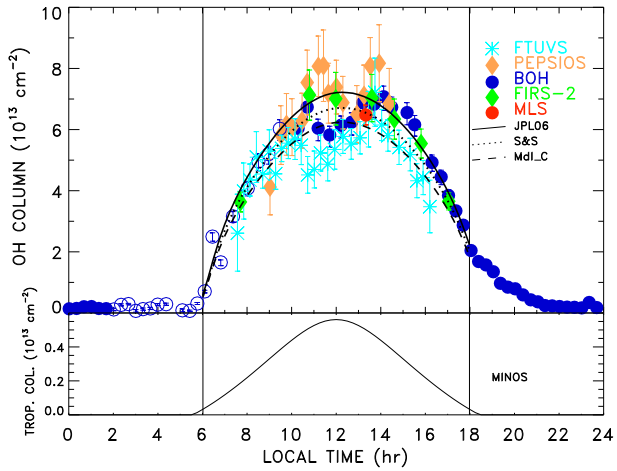

Figure 15. Comparison of OH columns for September 23, 2004.

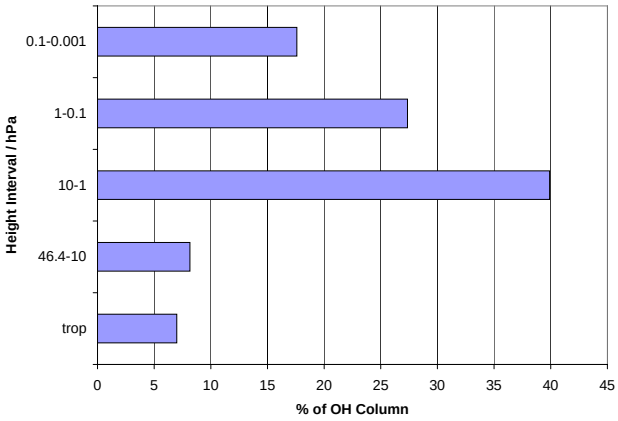

Figure 16. Contribution of different height intervals to the total OH column.

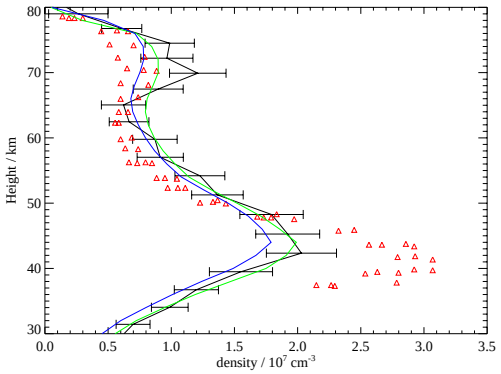

Figure 17. MLS OH altitude profiles compared with MAHRSI. The black line is a zonal average of OH profiles from MLS For September 7, 2005. The error bars for MLS OH include precision and systematic errors (2-σ). The MAHRSI data for August 15, 1997 is denoted by red triangles. The latitude range (12–32°S, 33–53°N) for the MLS zonal average was chosen so that the SZA range matches the MAHRSI SZA range (32–49°). Model C profiles are shown for SZA = 32° (green) and SZA = 49° (blue).

Tables

Table 1. Target molecule line-center frequencies for MLS HO_x bands

Band	Molecule	Frequency / GHz
15, 18	OH	2514.317
16, 19	OH	2509.949
16, 19	O_3	2509.560
17, 20	O_2	2502.324
17, 20	O_3	2543.208
28	HO_2	649.702
30	HO_2	660.486

Table 2. Meaning of bits in the 'Status' field.

Bit	Value[a]	Meaning
0	1	Flag: Do not use this profile (see bits 8–9 for details)
1	2	Flag: This profile is 'suspect' (see bits 4–6 for details)
2	4	Unused
3	8	Unused
4	16	Information: This profile may have been affected by high altitude clouds
5	32	Information: This profile may have been affected by low altitude clouds
6	64	Information: This profile did not use GEOS-5 temperature a priori data
7	128	Unused
8	256	Information: Retrieval diverged or too few radiances available for retrieval
9	512	Information: The task retrieving data for this profile crashed (typically a computer failure)

[a] 'Status' field in L2GP file is total of appropriate entries in this column.

Table 3. Summary of precisions, resolution, and uncertainties for the MLS OH product

Region	Precision[a] / 10^6 cm^{-3}	Resolution Vert. × Horiz. / km	Bias uncertainty / 10^6 cm^{-3}	Scaling uncertainty / %	Comments
<0.003 hPa	—	—	—	—	Unsuitable for scientific use
0.003 hPa	0.6	5.0 × 220	0.034	90.	
0.01 hPa	1.3	2.5 × 200	0.031	41.	
0.1 hPa	4.2	2.5 × 180	0.12	3.1	
1.0 hPa	2.4	2.5 × 165	0.50	7.	
10 hPa	8.0	2.5 × 165	0.18	1.5	
32–10 hPa	20.0	2.5 × 165	0.50	1.3	Use day–night difference
1000–32 hPa	—	—	—	—	Unsuitable for scientific use

[a] Precision on individual profile

Table 4. Summary of precisions, resolution, and uncertainties for the MLS HO_2 product

Region	Precision[a] / 10^6 cm^{-3}	Resolution Vert. × Horiz. / km	Bias uncertainty / 10^6 cm^{-3}	Scaling uncertainty / %	Comments
< 0.03 hPa	—	—	—	—	Unsuitable for scientific use
0.046 hPa	9.	16 × 600	0.39	22.	Use day–night difference
0.10 hPa	16.	16 × 400	0.46	16.	Use day–night difference
1.0 hPa	18.	5.5 × 660	1.1	6.	Use day–night difference
10. hPa	8.	4.5 × 450	37.	20.	Use day–night difference
1000–21 hPa	—	—	—	—	Unsuitable for scientific use

[a] Precision on individual profile